Computational Investigation of Nominally-Orthogonal Pneumatic Active Flow Control for High-Lift Systems

Seyedeh Sheida Hosseini* , C. P. van Dam†
University of California Davis, Davis, CA 95616
Shishir A. Pandya‡
NASA Ames Research Center, Moffett Field, CA 94035

We explore the feasibility of using nominally-orthogonal jets as active aerodynamic load control for multi-element high-lift systems, and whether the nominally-orthogonal jets can offer a variety of performance improvements. These nominally-orthogonal jets inject momentum normal to the airfoil surface near the flap trailing edge, where they create a vortex that entrains flow from the opposing side and change the airfoil circulation. Lift-enhancement opportunities of trailing edge nominally-orthogonal jets have previously been studied by Malavard et al.[1] and Blaylock et al.[2,3] on single-element airfoils; however, their effect on drag was not thoroughly investigated. In this study, we investigate two-dimensional nominally-orthogonal jet effects on both lift and drag on a two-element airfoil, NLR7301. We utilize Chimera Grid Tools to generate structured curvilinear overset grids, and the Reynolds-averaged Navier-Stokes solver OVERFLOW-2 to solve for the flow field around the airfoil. We perform various computational sensitivity studies on the baseline airfoil without a jet to validate computational results against benchmark experimental data. Using a Chimera overset grid topology, we demonstrate a similar lift-enhancement effect between a nominally-orthogonal jet and a nominally-orthogonal physical tab employed at the same location on the studied airfoil. After we introduce the nominally-orthogonal jet concept, we investigate nominally-orthogonal jets with various momentum coefficient settings, $C_\mu = 0.00 - 0.04$ and present a lift-enhancement relationship $\Delta C_l \simeq 3.59\sqrt{(C_\mu)}$ for this airfoil. We discuss that utilizing a nominally-orthogonal jet with $C_\mu = 0.01$ can shift the linear region of the lift curve by a $\Delta C_l = 0.36$ for the pressure side jet and by a $\Delta C_l = -0.27$ for the suction side jet. Employing a nominally-orthogonal jet is also shown effective in altering the drag. To study the impact, we carry out a drag decomposition study in the form of drag polars. We show for a given $C_l = 2.50$, a nominally-orthogonal jet with $C_\mu = 0.01$ on the pressure and suction side of the airfoil results in 113 drag count decrements and 41 drag count increments, respectively, compared to the baseline airfoil with no jet. These results show that large and controllable changes in aerodynamic performance can be achieved by relatively small active flow control inputs using the nominally-orthogonal jets presented in this study.

Nomenclature

α	Angle of attack	$\dot{m}$	Mass flow rate
c_{flap}	Flap chord	M	Mach number
c_{ref}	Reference chord	Re	Reynolds number
C_d	Drag coefficient	S_t	Strouhal number
C_l	Lift coefficient	U_∞	Freestream velocity
C_μ	Microjet momentum coefficient (Equation 1)	U_j	Microjet velocity
DT	Physical time step	ρ	Density
hj	Microjet cross sectional size		

*Graduate Student Researcher, AIAA Student Member.
†Professor & Associate Dean, Associate Fellow AIAA.
‡Research Scientist, AIAA Senior Member.

I. Introduction

The primary goal of a high-lift system design is to control lift (and drag) through a careful design of leading and trailing edge surfaces to achieve high performance at takeoff and landing with minimal impact on cruise C_D.[4] High-lift systems have a significant impact on the sizing, economics, and safety of transport airplanes. An optimal wing design for efficient flight is challenging as airplanes operate over a wide range of airspeeds and altitudes. The performance is mostly dictated by the stall speed and lift-to-drag ratio with the design challenge of achieving high-lift high maximum lift coefficient ($C_{L_{max}}$) during high-lift conditions (i.e. takeoff and landing) while minimizing the drag coefficient (C_D) during cruise.[5]

An increase of 1.0% in $C_{L_{max}}$ results in an increased payload of 22 passengers or 4400 lb for a fixed approach speed for landing, and an increase of 1.0% in lift-to-drag ratio during takeoff results in a payload increase of 14 passengers or 2800 lb for a given range of a large twin-engine aircraft.[6] Takeoff and landing only last for a few minutes and the airplane is in cruise for most of its service time. Thus, improving low-speed performance requires careful consideration of the impact on cruise performance, weight, complexity, and capital and operational expenditures.

Active Flow Control (AFC) is a technology with the potential to adaptively and rapidly change aerodynamic characteristics without the use of large, slow, conventional control surfaces such as flaps and slats in a high-lift system. Current AFC research for high-lift systems tends to focus on nominally-tangential jet blowing to mitigate boundary layer separation.[7–10] In the present study, we investigate low-momentum nominally-orthogonal pneumatic jets as applied close to a flap trailing edge of a multi-element airfoil as a possible mechanism to control aerodynamic loads and performance.

Active Flow Control can be studied in three domains: flow phenomena, control/sensors, and actuators/devices.[11] Flow phenomenon investigations are often the first step prior to the design of controls/sensors and actuators/devices (See Figure 1). High-lift active flow control studies with the focus on flow phenomena are generally directed towards two major categories: separation mitigation and aerodynamic load control. The effects, however, are not necessarily exclusive; improving one category can have positive and negative effects on the other one. Therefore, the objective is to choose an AFC approach which attains an overall favorable performance while minimizing trade-offs.

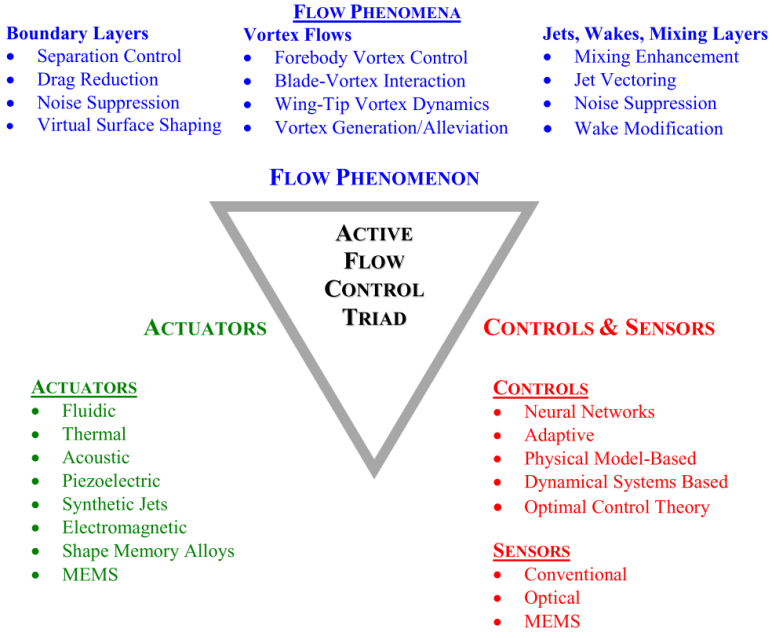

Figure 1: Active flow control domains adapted from Kral.[11]

For separation mitigation, various technologies such as vortex generator (VG) jets,[12] smart VGs,[13] plasma actuators,[14] blowing and suction,[15] and synthetic jets[16] have been studied. All the mentioned devices mitigate flow separation by introducing high-momentum to the flow in the boundary layer or removing low

momentum fluid from the boundary layer. The velocity of the boundary layer near the wall over an airfoil is relatively slower than the outer layer; therefore, the flow in the boundary layer is highly affected by the pressure gradient. The addition of momentum in the desired direction of the flow therefore delays separation, and adds a small amount of camber.

Historically, passive VGs[17] have been used to re-energize the flow to delay separation at the cost of adding drag during cruise. In contrast to passive VGs, active separation mitigation does not encounter cruise drag as it is only employed when needed at low-speeds. Nominally-tangential surface blowing has been extensively researched in the last decade for a variety of aerodynamics-related applications such as leading-edge separation mitigation for closely-coupled engine integration,[18] outer-wing stall mitigation,[10] trailing-edge separation mitigation,[8,9,19–21] and enhanced control authority of a vertical tail.[22] Some of the baseline geometries selected to study nominally-tangential surface blowing have highly separated profiles to start with; for example, the two element DLR-F15 airfoil used by Bauer et al.[23] has a flap with highly separated flow.[24] Therefore, the integrated impact of nominally-tangential surface blowing on the current commercial aircraft high-lift systems (especially the flap configurations) with mainly attached flow profiles is not clear in view of AFC energy requirements.

For aerodynamic load control, modifications to the flow at the trailing edge are required. Various design concepts have been investigated such as circulation control wings,[25] adaptive compliance wings,[26] miniature trailing-edge effectors,[27] microtabs,[28–31] and microjets.[2,3,32,33] In this AFC category, the flow at the trailing edge is altered and the airfoil effective camber is modified. Therefore, aerodynamic load control technologies are capable of increasing and decreasing the aerodynamic loads as needed. From the mentioned design concepts, small tabs perpendicular to the airfoil surface—so-called microtabs—are shown effective using two-dimensional studies for high-lift[33] and wind turbine blade applications.[28–31] These microtabs require mechanical actuation and volume space, and their deployment can lead to unfavorable transient effects. Chow and van Dam[30,34] have shown that as the tab deploys, a low pressure region behind the tab forms, which creates a vortex acting as a separation bubble. Once the tab is fully deployed, the bubble extends aft of the trailing edge and entrains flow from the suction side to the pressure side, achieving effective circulation control.

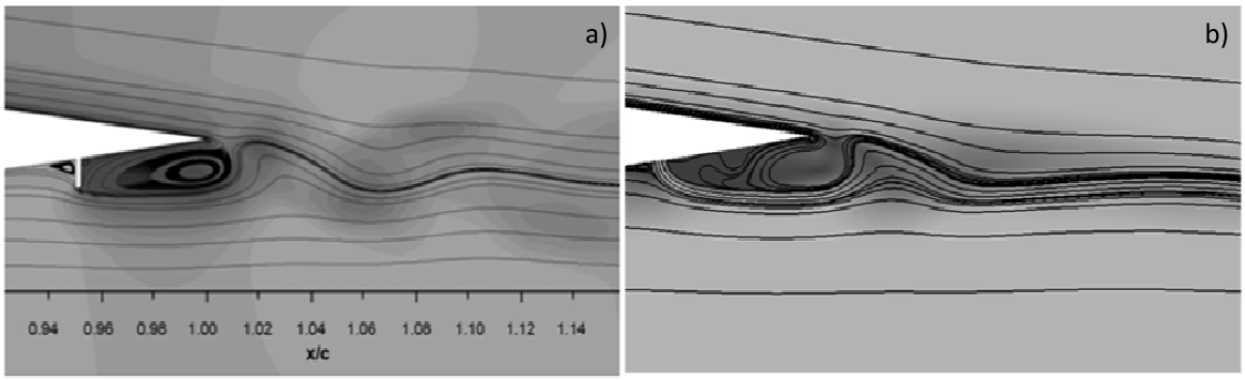

Figure 2: Adapted from Blaylock et al.[2] a) Streaklines for a fixed microtab case at $x/c = 0.95$, $\alpha = 0°$, $h_{tab} = 1.0\%$c, $Re = 1.0 \times 10^6$, $Ma = 0.25$ b) Streaklines for a constant microjet blowing case at $x/c = 0.95$, $\alpha = 0°$, $C_\mu = 0.003$, $h_{jet} = 0.5\%c$, $Re = 1.0 \times 10^6$, $M = 0.25$. Darker regions indicate lower pressures.

Small nominally-orthogonal pneumatic jets—so-called microjets—have been studied on single-element airfoils as an improvement to the microtab concept to replace the mechanical tab, to reduce space limitations, and to mitigate the transient effects.[2,3,32] Similar to microtabs, microjets modify the flow at the trailing edge (Figure 2). The term micro indicates that the topics discussed here are problems where a relatively small fluidic input can create a significant output through modifications at the flow near the airfoil trailing-edge.

A trailing edge jet on a single-element airfoil was initially studied as a means of circulation control by Malavard et al.[1] employing relatively high jet momentum, with C_μ values up to 1.6. In that study, Malavard et al.[1] suggested $\Delta C_l \propto \sqrt{(C_\mu)}$ as the lift enhancement correlation to the jet momentum coefficient. Recent two-dimensional numerical and experimental investigations on a single-element airfoil for wind turbine applications have shown that significant load control benefits can be obtained by relatively small jet momentum coefficients $C_\mu \leq 0.01$.[2,3,35,36]

This work demonstrates the effectiveness of nominally-orthogonal jets for improving the aerodynamic characteristics of high-lift flapped airfoils. In section II, we present the details of mesh and flow solver options, in section III, we preset the results of the AFC investigations and in section IV, we offer some concluding remarks.

In section II, we provide computational investigations on a two-element airfoil, NLR7301, at $\alpha = 6°$, $Re = 2.51 \times 10^6$ and $M = 0.185$ on the baseline airfoil with no microjet to best reproduce the experimental data presented by van den Berg and Gooden.[37] In section III, we place a uniform constant microjet with $C_\mu = 0.004$, at 95% of the flap chord on the airfoil flap's pressure side and we conduct a parallel study with a nominal physical tab (microtab) at 95% of the flap chord to compare microjet and microtab lift-enhancement effects. We investigate various microjet momentum coefficient settings, $C_\mu = 0.00 - 0.04$, on the airfoil flap's pressure side. Further, we address how microjets effect the lift and drag curves in detail and provide a drag decomposition study.

II. Computational Setup Prior to Microjet Activation

The NLR7301 airfoil is the selected multi-element airfoil for its availability of benchmark experimental data.[37] The experimental pressure coefficient profile was provided for an angle of attack $\alpha = 6°$ alongside a range of lift and drag coefficient values at $Re = 2.51 \times 10^6$ and $M = 0.185$. The experimental accuracy for the lift coefficient was $\pm 0.4\%$, for the drag coefficient was $\pm 2\%$, and for the surface pressure coefficients was $\pm 0.5\%$.[37] The normalized airfoil geometry is shown in Figure 3 where the cruise reference chord, c_{ref}, is 1.

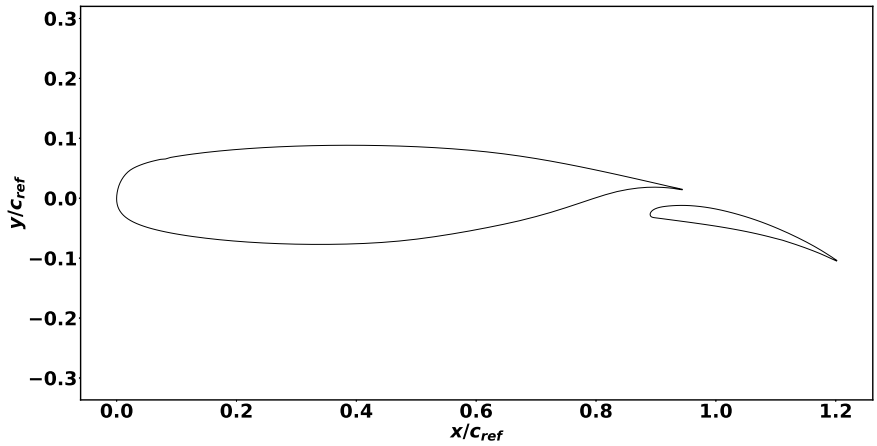

Figure 3: Airfoil surface grid definition. 20° flap deflection, $0.053c_{ref}$ overlap, and $0.026c_{ref}$ gap.

II.A. Surface Grid Definition Sensitivity

To begin the computational setup, we perform a surface definition sensitivity study at $\alpha = 6°$ with the following specifications: O-grid topology around the airfoils with a Cartesian far-field grid growing to 50 chord lengths, PEGASUS[38] mesh connectivity software, central difference and ARC3D diagonalized approximate factorization[39] schemes for the Navier-Stokes equations, and the SA turbulent model.[40] The surface definition sensitivity matrix is given in Table 1.

We study the surface definition sensitivity using both the comparison of the pressure coefficient profiles and the overall force integrations. All the pressure profiles are found to be in good agreement at $\alpha = 6°$ with the published experimental data[37] suggesting no difference between the various studied cases. The effect of surface definition refinement on the integrated lift and drag coefficient values, Figure 5, shows that the increase of the grid resolution leads to 0.2% improvement for the lift coefficient and a 1.25% improvement for the drag coefficient which both are smaller than the reported[37] experimental accuracy. The computed drag coefficient for all the cases is larger than the experimental one. This can be explained due to using the fully turbulent simulation, whereas the experiment was conducted with natural transition, and the published computational INS2D study employed a transition model[41] as well. The improvement in the drag coefficient

Table 1: Surface grid sensitivity matrix. Each value represents the number of grid points used to define the corresponding surface.

	Main Element	Flap Element
Coarse	600	300
Medium	800	400
Fine	1000	500
Extra fine	1200	600

ceases with the increase of surface points. Therefore, we select a surface definition of 1000 points on the main element and a surface definition of 500 points on the flap element for the remainder of this study.

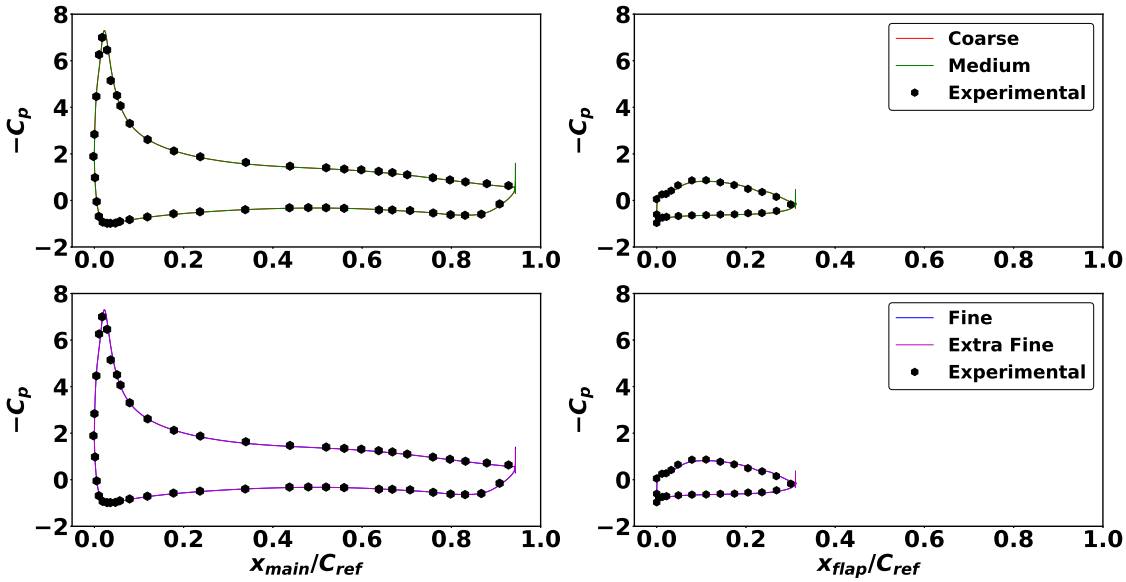

Figure 4: Pressure profile comparisons for various surface definitions at $\alpha = 6°$, $Re = 2.51 \times 10^6$ and $M = 0.185$. All studied surface definitions are in good agreement with the published experimental data.[37]

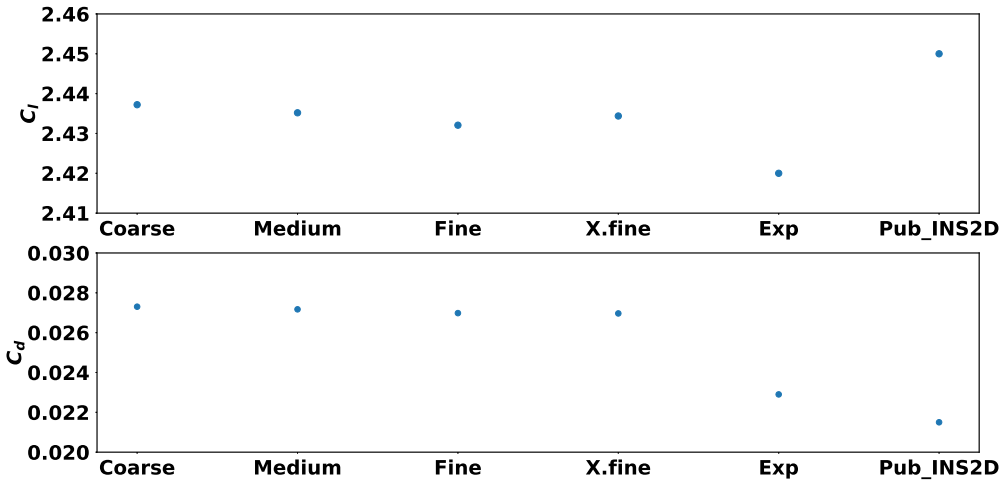

Figure 5: Lift and drag coefficients for various surface definition setups in comparison with the experimental data[37](Exp) and a previous numerical study[41](Pub_INS2D).

II.B. Volume Grid Sensitivity

A typical characteristic of multi-element airfoils is the presence of wakes and shear layers from upstream elements near the downstream elements. Therefore, grid refinement is necessary to capture the flow physics more accurately. We generate vorticity contours to guide the off-body volume grid refinement process (Figure 6). We perform grid refinement in steps: initially, we add a shear layer grid and a wake grid individually to the baseline grid; then we add them both together to study the combined effects (Figure 7).

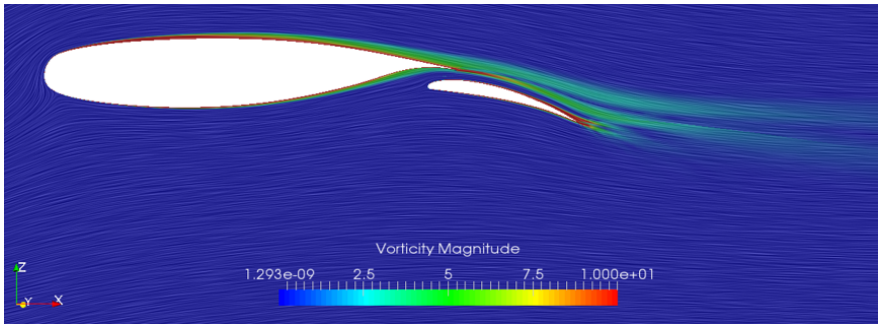

Figure 6: Vorticity contours provide insights to shear layer and wake profiles.

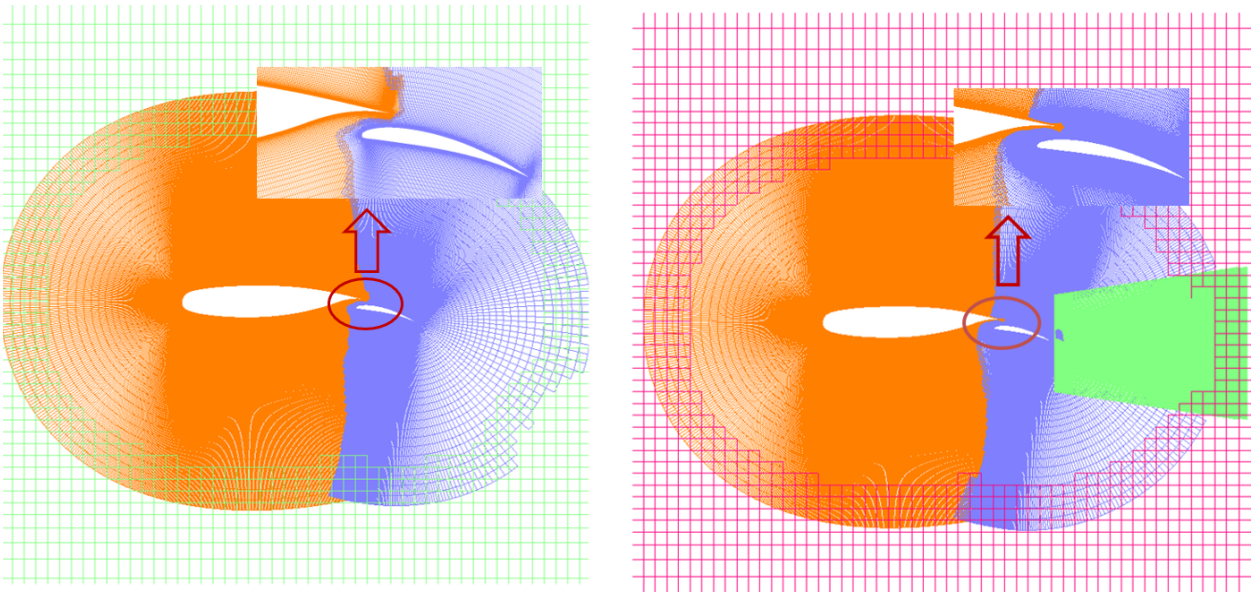

Figure 7: Grid refinement to capture flow field details. Left: baseline, right: shear and wake grid added.

Table 2: Lift and drag coefficient sensitivities to grid refinement.

	C_l	C_d
Baseline	2.4321	0.0270
Grid refinement for shear layer	2.4371	0.0267
Wake layer grid addition	2.4325	0.0268
Both shear layer refinement and wake grid addition	2.4356	0.0266
Experimental	2.42	0.0229

Table 2 suggests that the grid refinement for shear layer and the wake grid both increase the accuracy of the simulations, and the impact of both can be superposed. The integrated lift coefficient is not highly affected by the addition of the refinement grids as all the obtained values are within the reported accuracy

of the experimental data. However, the computed drag coefficient is improved, which suggests that the drag coefficient is more sensitive to the shear and wake grid refinement than the lift coefficient. We select the fine surface grid with both the shear layer and the wake grid for the remaining study.

II.C. Grid Connectivity Sensitivity

We investigate the grid connectivity using two different approaches starting from identical grids (see Figure 8). Initially, we utilize PEGASUS[38] for its automated hole cutting capabilities. PEGASUS's automation process minimizes user interface and therefore customization. PEGASUS is a stand-alone tool and it lacks the capability of hole cutting for moving or adaptive grids which may be required for future work. To have more grid customization power, we employ hole-cutting with DCF (Domain Connectivity Function) routines[42] readily available in the OVERFLOW solver in a parallel study. DFC hole cutting requires significant user inputs; however, it is capable of hole cutting for moving or adaptive grids.

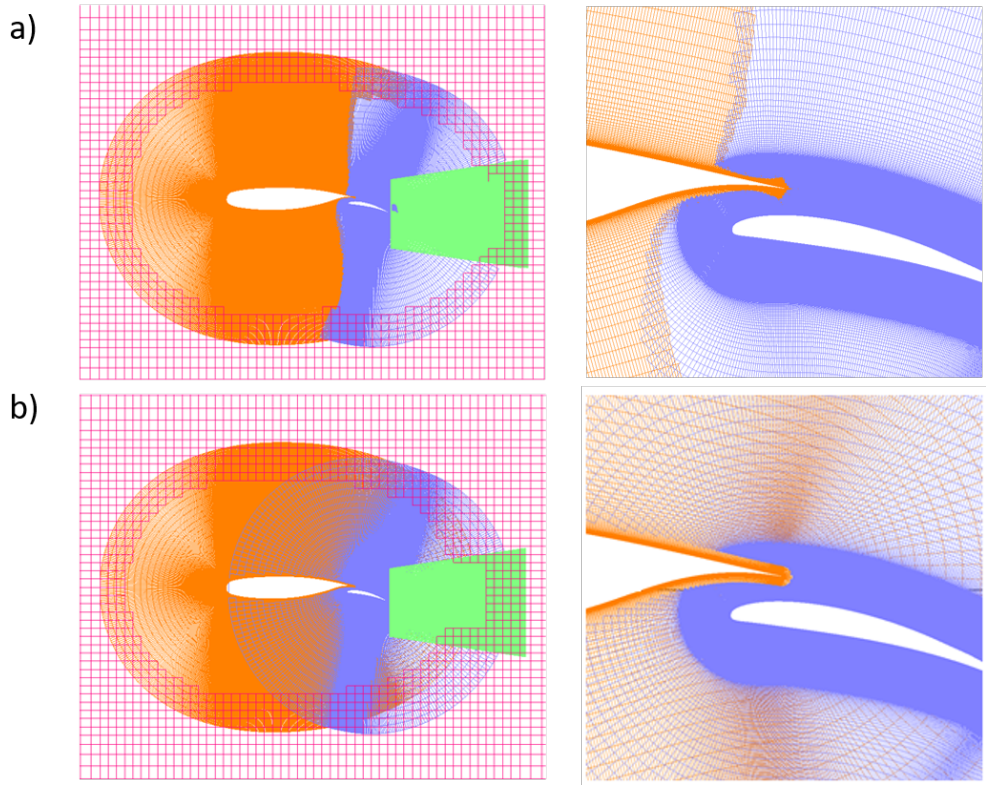

Figure 8: Sensitivity to overset mesh connectivity. a) PEGASUS grid, b) DCF grid.

Table 3: Lift and drag coefficient sensitivities to the two studied overset approaches. $\Delta\%$ is with respect to the reported experimental data[37] at $\alpha = 6°$.

	C_l	$\Delta C_l\%$ error	C_d	$\Delta C_d\%$ error
PEGASUS	2.436	0.65%	0.0266	16.2%
DCF	2.413	0.30%	0.0289	26.2%

As we are looking to obtain lift and drag coefficient differences between no-jet and microjet cases, it is important to stay consistent in how the grid connectivity is performed for each case. Therefore, we choose DCF hole cutting to create consistent grids for this study. Once we select the overset approach, we modify the grid further to better suit the upcoming microjet study. The flap grid is broken in two parts, one part

containing the majority of the flap surface and one part containing a small surface close to the flap trailing edge. The off-body grids are modified to be denser near the surface and gradually coarsen away from the bodies. The final grid has 755749 vertices in two-dimensions with maximum y^+ wall spacing of 3.65. The grid modifications, shown in Figure 10, improves the accuracy of the lift and drag coefficient values; the lift coefficient is updated to 2.416 (ΔCl% of 0.16%) and the obtained drag coefficient is updated to 0.0284 (ΔCd% of 24.0%).

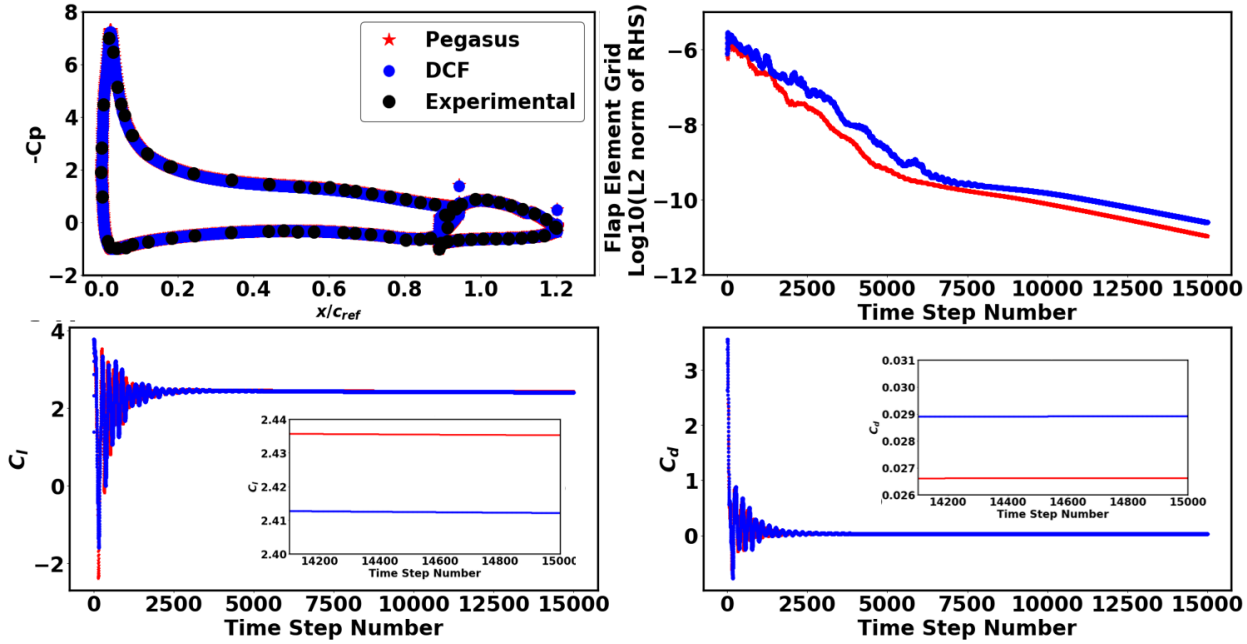

Figure 9: Overset mesh-connectivity sensitivity. Both approaches have similar convergence behavior.

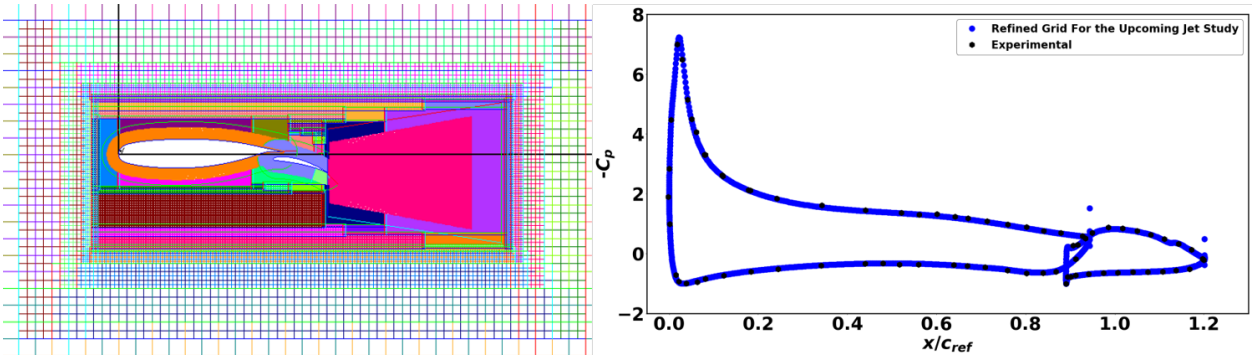

Figure 10: Left: grid modification to prepare for the upcoming microjet study. The flap grid is broken into two pieces, green grid is to allow for microjet activation and the purple grid is for the remainder of the flap. Right: Pressure profile.

II.D. Solver Sensitivity

After finalizing the grid, we perform a solver sensitivity study. We investigate the combinations of two Right Hand Side (RHS) schemes, i.e. central difference and HLLE+ upwind,[43] with three Left Hand Side (LHS) schemes of ARC3D approximate factorization,[44] ARC3D diagonalized approximate factorization[39] and SSOR algorithm for the Navier-Stokes equations using 48 Haswell processors per case study on NASA's Pleiades supercomputer. Various solver combinations are given in Table 4. Data presented in Table 4 indicate that the solvers considered here provide similar integrated force values. The RHS scheme choice is shown to have

the dominant effect on the accuracy of the results, while the LHS schemes play the main role in determining the wall clock time depending on the number of required operations the scheme holds. The convergence level in form of L2 norm of residual for cases 00, 20, and 26 was similar and about two orders of magnitude higher compared to cases 60 and 66. We select case 02, central difference for RHS and ARC3D approximate factorization for LHS, for the remainder of the study as it is shown to have the shortest wall clock time and is one of the more accurate schemes.

Table 4: Solvers of study in comparison in terms of wall clock time and force coefficients at $\alpha = 6°$. $\Delta\%$ is relative to the reported experimental data.[37]

Case	LHS	RHS	Clock time[min]	C_l	$\Delta C_l\%$ error	C_d	$\Delta C_d\%$ error
00	ARC3D approx. factor.	Central diff.	27.30	2.4159	0.16%	0.0284	24.0%
20	ARC3D diag. approx. factor.	Central diff.	16.38	2.4159	0.16%	0.0284	24.0%
60	SSOR	Central diff.	39.11	2.4159	0.16%	0.0284	24.0%
26	ARC3D diag. approx. factor.	HLLE++ upwind	23.21	2.4276	0.31%	0.0286	24.9%
66	SSOR	HLLE++ upwind	42.14	2.4276	0.31%	0.0286	24.9%

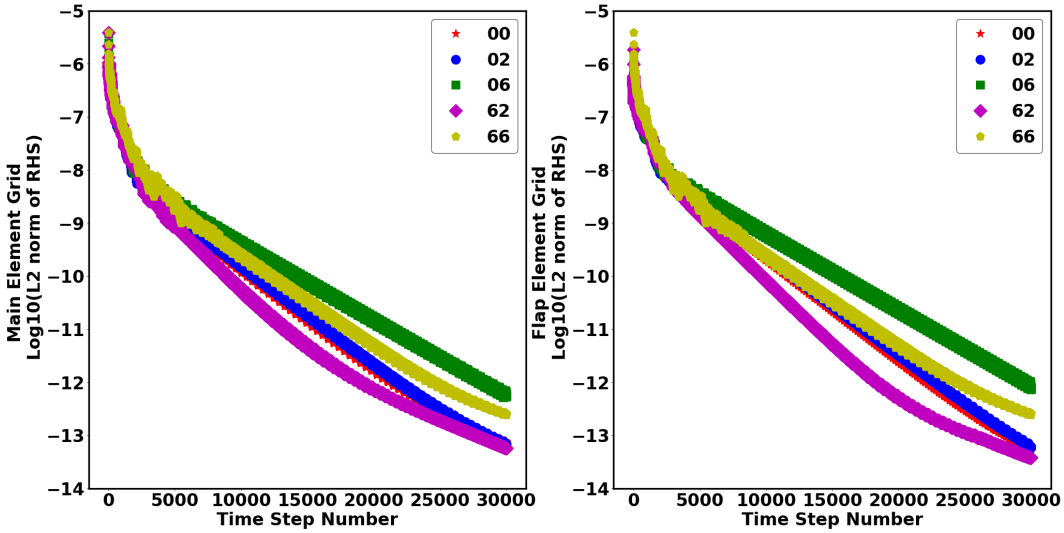

Figure 11: Convergence behavior of different solvers.

II.E. Turbulence Model Sensitivity

All the prior sensitivities in this study employed the fully turbulent SA[40] model; therefore, we investigate two additional models of fully turbulent SST[45] and SST with Langtry-Menter transition.[46]

Table 5: Turbulence model sensitivity study in terms of wall clock time and force coefficients at $\alpha = 6°$.

Turbulence model	Clock time[min]	C_l	$\Delta C_l\%$ error	C_d	$\Delta C_d\%$ error
SA	16.38	2.4159	0.16%	0.0284	24.0%
SST	32.08	2.3946	1.05%	0.0301	31.4%
SST with Langtry-Menter transition	52.35	2.4609	1.69%	0.0260	13.5%

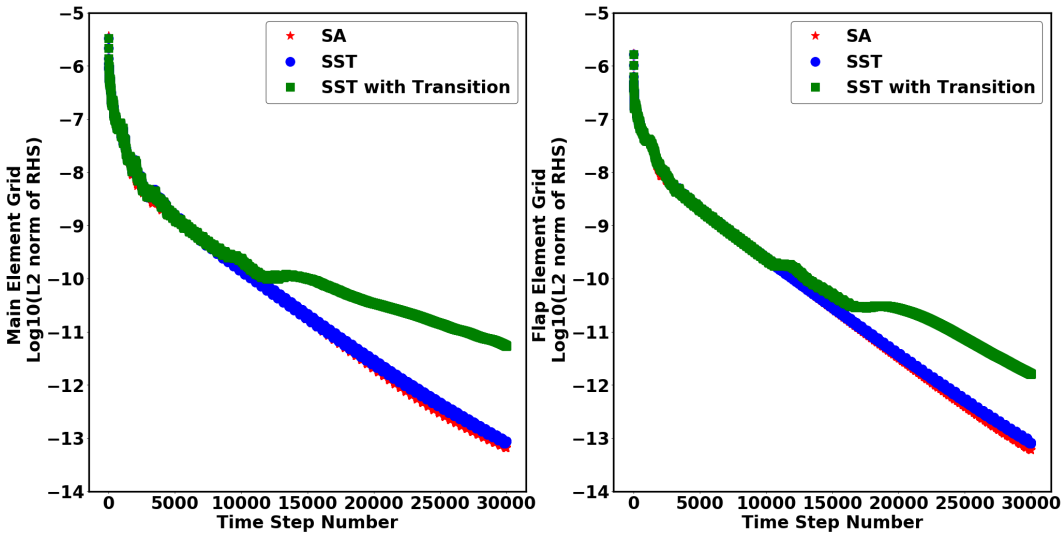

Figure 12: Convergence behavior using various turbulence models at $\alpha = 6°$.

Data presented in Table 5 indicates that the SA model results in the most accurate lift coefficient compared to the other two models; whereas, the SST with Langtry-Menter transition model results in the most accurate drag coefficient. All three models provide acceptable convergence levels, the convergence level is similar for SA and SST models and slightly better than the SST with transition model (Figure 12). To study the turbulence modeling effect on the microjet study (explained in the next section), we perform a sensitivity study for a microjet with $C_\mu = 0.01$. We observe that the SA model in our study results in steady flow behavior, whereas the SST model results in an unsteady flow behavior. This is also consistent with the assertion in the literature[47] that the SA model can overdamp some unsteady flows. We select the SST model for the upcoming microjet study to avoid hiding possible unsteadiness in the flow field. In the future studies we will investigate the microjet effects using SST with Langtry-Menter transition model.

III. Computational Investigation of Flap Microjet's Aerodynamic Impact

A microjet can be characterized by the ratio of the momentum within the microjet to the freestream momentum, known as momentum coefficient C_μ

$$C_\mu = \frac{\dot{m}_j U_j}{\frac{1}{2}\rho_\infty U_\infty^2 A_{ref}} \tag{1}$$

where $\dot{m}_j$ is the mass flow rate of the jet, U_j is the averaged velocity of the jet measured at the exit, ρ_∞ is the freestream density, U_∞ is the freestream velocity, and A_{ref} is the airfoil reference area. For two-dimensional and incompressible flow, Equation 1 reduces to Equation 2.

$$C_\mu = 2\frac{U_j^2 h_j}{U_\infty^2\ c_{ref}} \tag{2}$$

We model the microjet as a surface jet with a constant velocity, U_j, across the microjet exit, h_j, centered at 95% of the flap chord. We implement the microjet using a boundary condition within OVERFLOW that specifies the ratio of the microjet velocity to the freestream velocity. We set the nominal microjet exit width, h_j, to 0.005 (0.5% c_{ref}) and we carry out the study at $Re = 2.51 \times 10^6$ and $M = 0.185$, which correspond to the conditions the experiment[37] was performed for the baseline airfoil (no jet).

III.A. Microjet vs. Microtab Proof of Concept

As mentioned in the introduction, the microjet concept was studied for single-element wind turbine applications[2] as an alternative to microtabs. Considering microtabs were examined for two-dimensional high-lift system applications,[33] we desire to have a comparison between the two concepts in this study. Therefore,

we modify the microjet grid to accommodate a nominal microtab with dimensions of $1\%c_{ref}$ length and $0.2\%c_{ref}$ width centered at $95\%c_{flap}$ (Figure 14). Because the numerical results are validated at a representative angle for takeoff condition $\alpha = 6°$, we perform comparison studies at $\alpha = 6°$. We perform a sensitivity study with varying C_μ for the microjet case and find that the required microjet C_μ is 0.004 in order to provide the same lift value provided by the microtab (see Table 6). Both technologies lead to lift enhancement due to increase in circulation. They are shown to modify the suction peak as a result of generating two counter-rotating vortices that entrain flow around the flap trailing edge (Figure 14). While the lift values for both of the configurations are the same, the drag value for the airfoil with microjet is smaller than the airfoil with microtab, a similar trend to the one observed by Blaylock et al.[2] We also observe that incorporating a microjet on the baseline airfoil leads to a lower drag coefficient value compared to the baseline airfoil with no active flow control. In 1956, Malavard et al.[1] showed variations in drag using trailing edge jets. To the best of our knowledge the effects of trailing edge nominally-orthogonal jets on drag have not been investigated in details in literature. We discuss the drag reduction characteristics in detail in section III.C.

Table 6: Force coefficient comparison with respect to the baseline with no AFC at $\alpha = 6°$.

	C_l	C_d
Baseline (no AFC)	2.395	0.0301
Microtab	2.626	0.0358
Microjet ($C_\mu = 0.004$)	2.627	0.0284

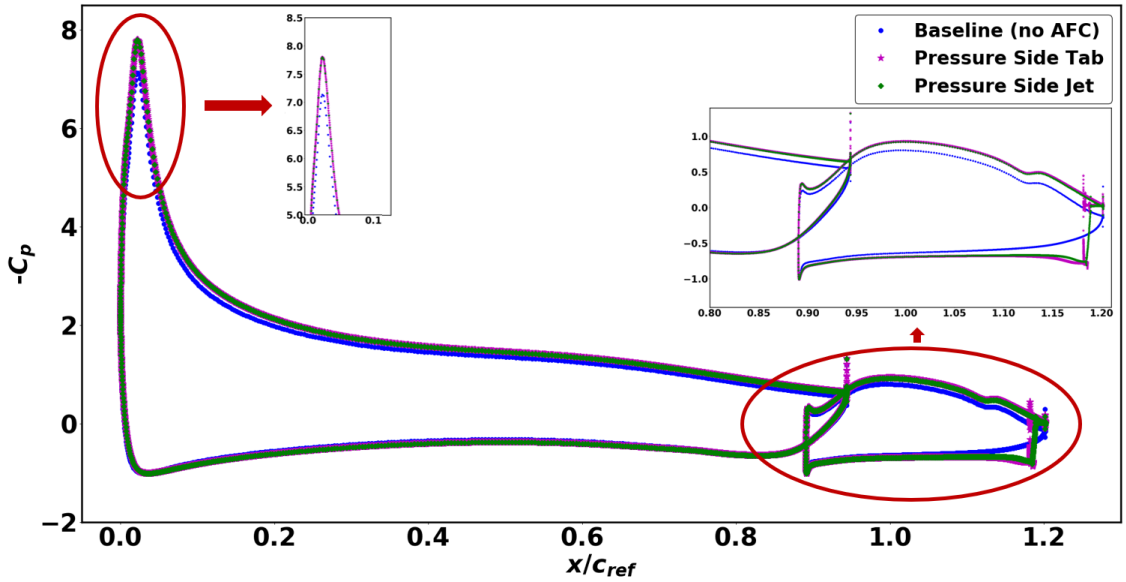

Figure 13: Pressure profile comparison for a fixed microtab and a constant blowing microjet at $\alpha = 6°$, $Re = 2.51 \times 10^6$ and $M = 0.185$. The profiles match well, generating the same lift level.

III.B. Momentum Coefficient Sensitivity

We investigate the effects of various microjet momentum coefficient settings, $C_\mu = 0.0004 - 0.04$, on the lift and drag coefficients for a microjet on the pressure side at $\alpha = 6°$. For momentum coefficients below 0.01, we observe that steady simulations are sufficient; however, for C_μ values greater and equal than 0.01, time-accurate simulations are necessary to obtain convergence due to unsteady flow behavior at this angle of attack. We perform time-accurate simulations using a dual time step approach[48] with 20 sub-iterations and a sufficiently small time-step for at least 100 time steps per period for $C_\mu \geq 0.01$.

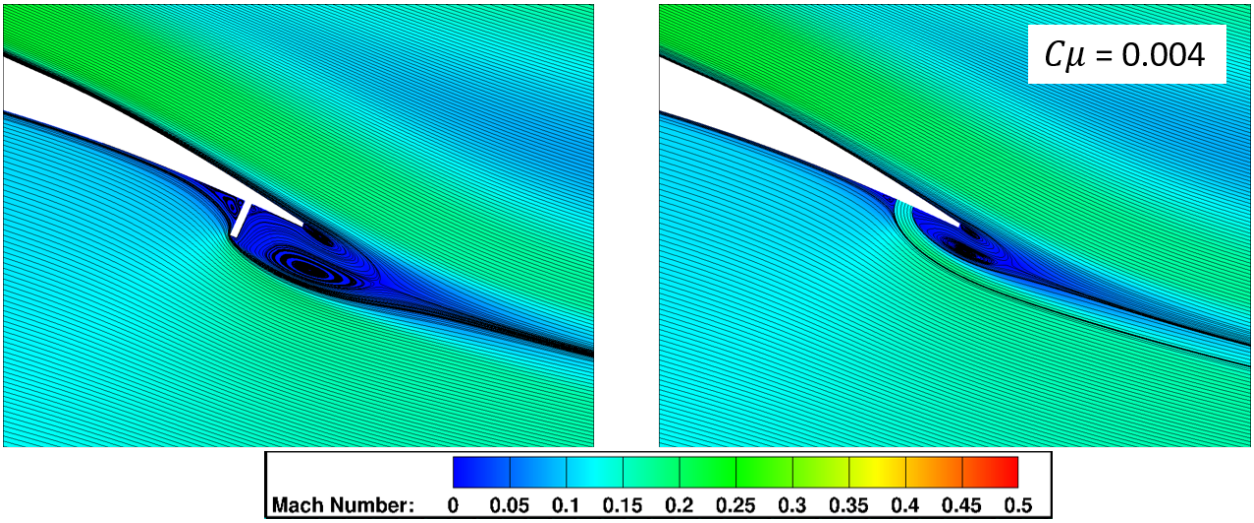

Figure 14: Streamlines for a fixed microtab on left and a constant blowing microjet on the right. Both approaches create two counter rotating vortices at the trailing edge as a mechanism to increase circulation.

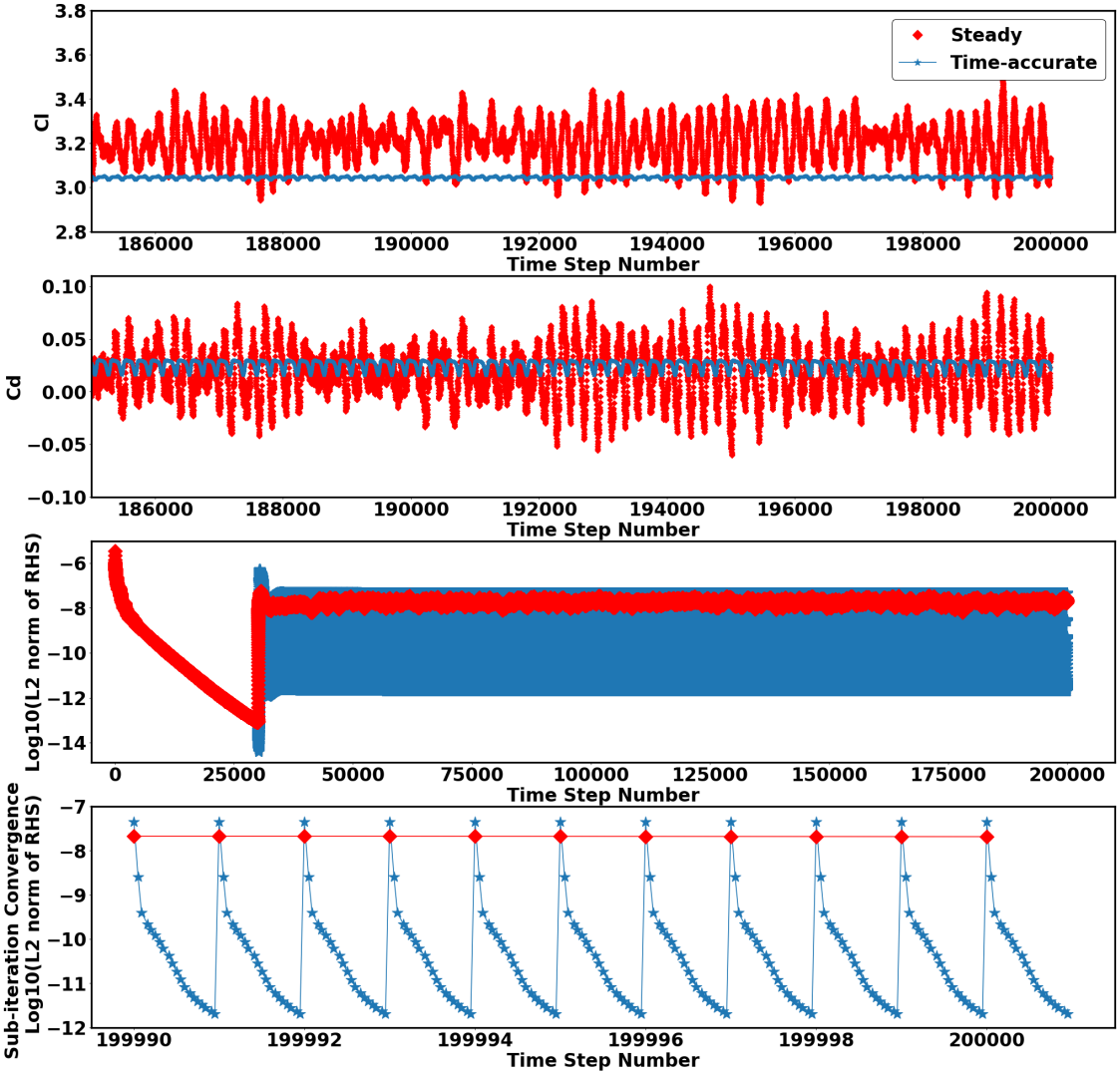

Figure 15: Steady vs. unsteady (time accurate) study for $C_\mu = 0.04$ at $\alpha = 6°$, $Re = 2.51 \times 10^6$ and $M = 0.185$. Microjet flow is started at 30001 time step.

Figure 15 compares the solutions for both the steady and unsteady simulations for $C_\mu = 0.04$. We can make a few remarks about this study: 1. We observe that the steady simulation leads to highly oscillatory force history values, the frequency and amplitude of the oscillations change with no repeating patterns; whereas the oscillations from the time-accurate simulations are all converged with a repeating pattern. The running-average standard deviation for the last ten full periods of the force history using the time accurate solution are three orders of magnitude smaller than one lift count and one order of magnitude smaller than one drag count for the lift and drag coefficients respectively (see Figure 16). 2. The calculated average value from the time accurate simulations is well below and slightly above the average value calculated from the steady simulation for the lift and drag coefficients respectively. This suggests that a simple averaging over the steady force history does not lead to an equivalent averaging over the unsteady one (Figure 15), and thus we require unsteady simulations to obtain accurate results. 3. Once the microjet is turned on at the time step number of 30001, the L2 norm of residual drops only one order of magnitude in the steady simulation, oscillating back and forth suggesting that the solver is challenged to converge; whereas, the time accurate setup allows for about five orders of magnitude drop in L2 norm of the residual.

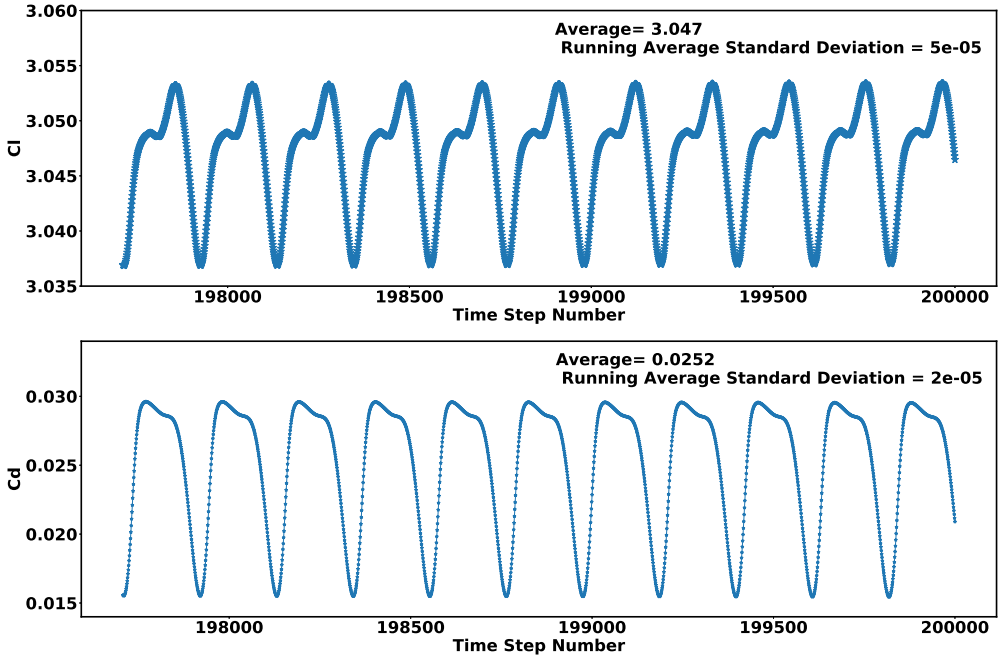

Figure 16: Last ten full oscillations force history for lift and drag coefficients for the time accurate simulation at $\alpha = 6°$, $Re = 2.51 \times 10^6$ and $M = 0.185$. The adequate running average standard deviation confirms a fully converged solution.

It is important to note that the flow unsteadiness is limited to small regions near the trailing edge of the flap and does not involve any large separation regions that could have invalidated the flow simulation results. Figure 17 illustrates vorticity flow visualization for three C_μ values of 0.004, 0.01, and 0.04, one steady and two unsteady cases. The two C_μ values of 0.01 and 0.04 create vortex sheddings with Strouhal numbers of 0.072 and 0.103 respectively.

Once the simulation convergence is assured, we study the effect of C_μ on lift and drag coefficients. Data presented in Figure 18 shows that as C_μ increases, C_l increases and C_d decreases; a 0.36 increment in the lift coefficient and a 0.0032 decrement in the drag coefficient are obtained at $C_\mu = 0.01$. The lift enhancement trend, $\Delta C_l \propto \sqrt{(C_\mu)}$, is similar to the one reported by Blaylock et al.[3] and Malvard et al.[1] Figure 18 further shows that the lift enhancement gradient becomes more and more flat as C_μ increases. This means that the increase in C_l is only marginal beyond a certain value of C_μ. We select a microjet with $C_\mu = 0.01$ for the remainder of this study.

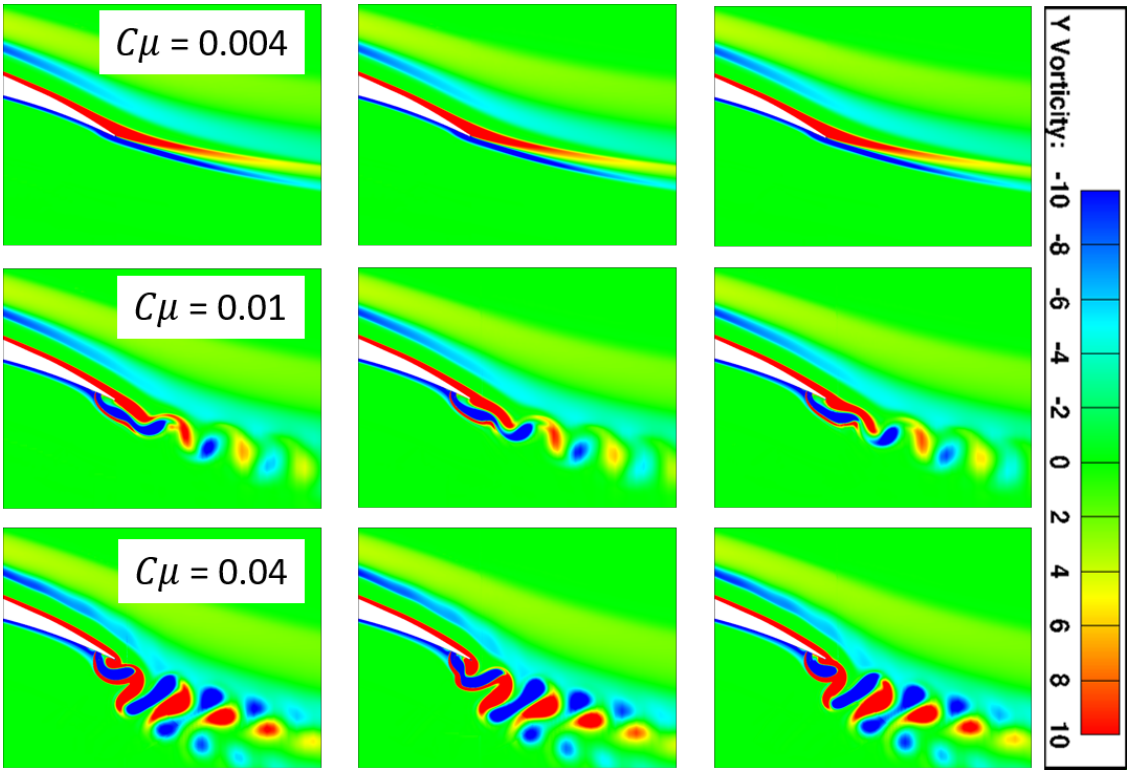

Figure 17: Left to right images correspond to vortex shedding from the maximum to the minimum peak at $\alpha = 6°$, $Re = 2.51 \times 10^6$ and $M = 0.185$. Microjet with $C_\mu = 0.004$ has steady flow and microjet with $C_\mu = 0.01$ and 0.04 creates a vortex shedding with Strouhal numbers of 0.072 and 0.103, respectively.

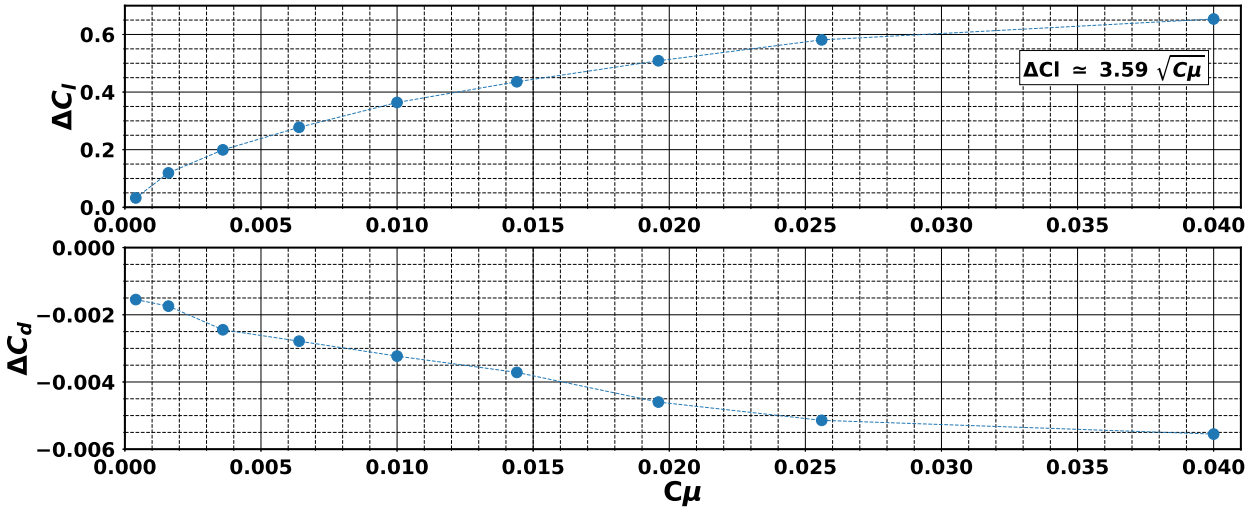

Figure 18: Microjet momentum coefficient effect on force coefficients at $\alpha = 6°$, $Re = 2.51 \times 10^6$ and $M = 0.185$.

III.C. Microjet Effect on Lift and Drag Curves

In this section we examine the predicted physics of the microjet with $C_\mu = 0.01$ and how it effects the flow over the studied airfoil at $Re = 2.51 \times 10^6$, $M = 0.185$. We investigate how the flow field over the airfoil changes as the angle of attack is increased and how the lift and drag coefficients reflect those changes (see Figure 19). The study suggests how microjets influence the circulation not by turning the trailing edge itself but rather by introducing flow orthogonal to the trailing edge (see Figure 22).

Thin airfoil theory explains that $\alpha_{L=0}$ is a function of airfoil camber and it decreases as the camber increases.[49] Although in this study, there is no inviscid assumption (as in thin airfoil theory), we expect the trends to be the same. Employing a microjet increases the flap's performance by altering the airfoil's effective camber, more negative $\alpha_{L=0}$ for the pressure side microjet, and more positive $\alpha_{L=0}$ for the suction side microjet. For a fixed $\alpha = 6°$ value, the microjet effect is seen in Figures 20 and 22. These figures reveal that the pressure side microjet moves the stagnation point downstream and the suction side microjet moves the stagnation point upstream. The change in the stagnation point changes the differential pressure between the upper and lower surfaces and therefore the generated lift.

We can further explain the circulation control effect for a given angle of attack by the magnitude of the suction peak, Figures 20 and 21. Employing a microjet can effectively alter the upstream flow on the leading edge of the main element. Utilizing a microjet with $C_\mu = 0.01$ is shown to shift the linear region of the lift curve by $\Delta C_l = 0.36$ for the pressure side microjet and by $\Delta C_l = -0.27$ for the suction side microjet (see Figure 19). The change in the lift coefficient is not simply due to the added momentum by the microjet. The lift control is rather done by altering the pressure field. At $\alpha = 6°$, the lift generated by the altered pressure field is found to be two orders of magnitude greater than the lift generated by the added momentum. To compare the effectiveness with a recent tangential blowing study on a single-element NACA0018 airfoil, a lift increment of 0.30 at $\alpha = 6°$ is reported by Eggert and Rumsey[21] with $C_\mu = 0.05$ which is five times higher than the C_μ employed in this study.

Incorporating the microjet on the pressure side alters the flow such that the velocity leaving the main element trailing edge is higher with pressure side microjet than the baseline (no jet). Thus the boundary layer can resist leading edge separation and increase the stalling angle slightly, known as the dumping effect.[4] For the suction side microjet, it is anticipated that the microjet creates a more favorable pressure gradient on bulk of the flap element, see Figure 21 at $x/c_{ref} = 0.97 - 1.10$, compared to the baseline (no jet) and thus it increases the stalling angle. In Figure 21, the main element leading edge pressure gradient appears to be smaller for both the pressure and the suction microjet compared to the baseline (no jet) and therefore they are expected to allow for a higher α_{stall} value. A close look at the trailing edge pressure behavior, Figures 20 and 21, suggests that the microjet affects the trailing edge pressure on the upper and lower surface of the airfoil similarly. Therefore, the main effect on the overall airfoil flow physics is dominated by the changes observed on the leading edge of the main element of the airfoil.

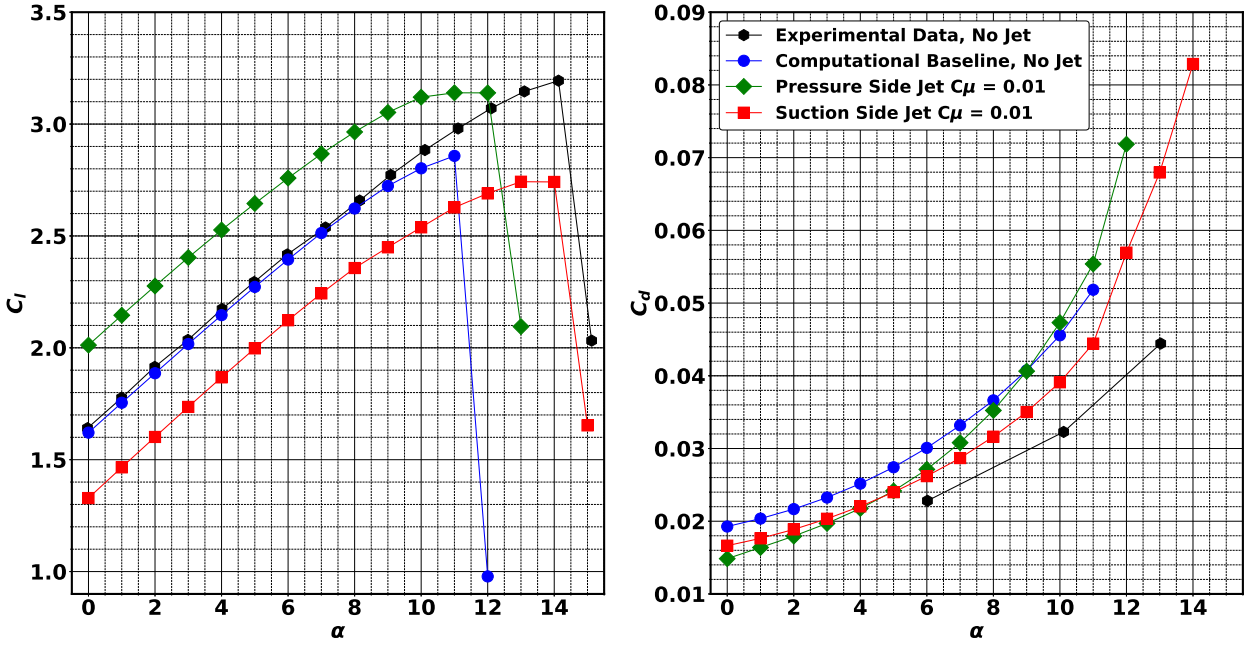

Figure 19: Microjet effect on the left: lift coefficient curve, on the right: drag coefficient curve at $\alpha = 6°$, $Re = 2.51 \times 10^6$ and $M = 0.185$.

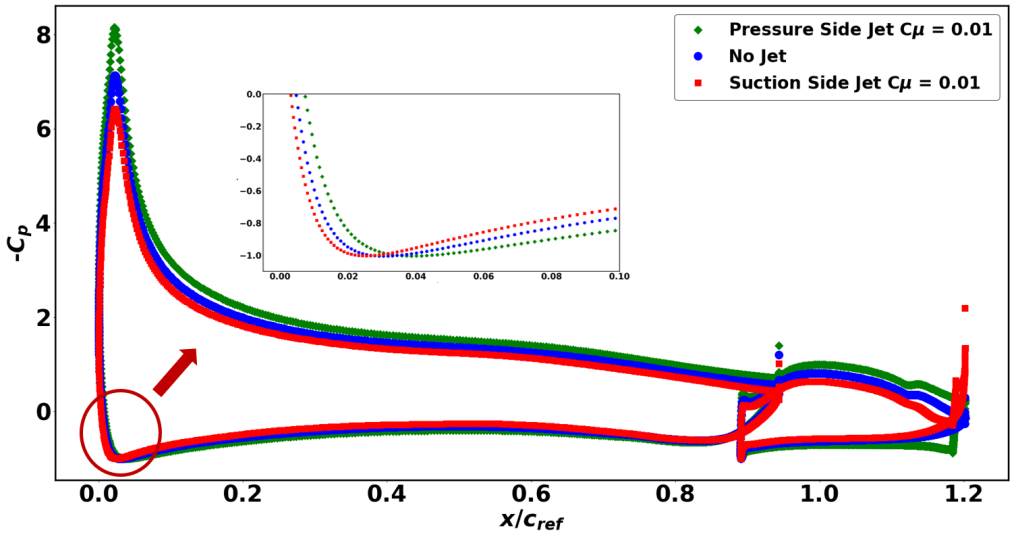

Figure 20: Microjet effect on the pressure profile at $\alpha = 6°$, $Re = 2.51 \times 10^6$ and $M = 0.185$.

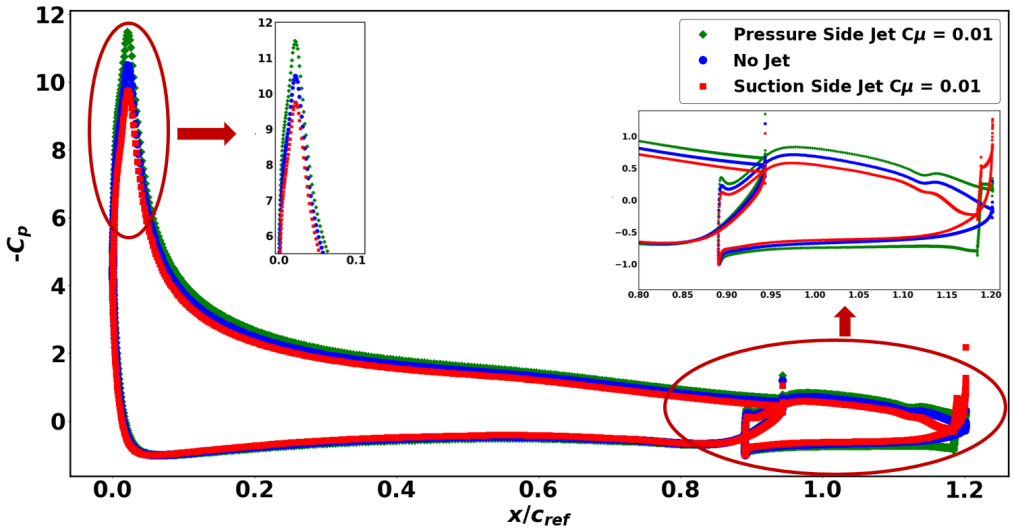

Figure 21: Microjet effect on the pressure profile at $\alpha = 11°$, $Re = 2.51 \times 10^6$ and $M = 0.185$.

The lift enhancement capabilities of pressure side jets on single element airfoils have been recognized before; in fact, they were recognized by Malvard et al.[1] in 1956; however, as mentioned earlier, the drag effect of a jet nominally-orthogonal to the surface on the pressure and suction side to the best of our knowledge has not been explained explicitly yet. In this study, we have shown that the microjet has noticeable impacts on the drag coefficient as well, Table 6, and Figures 18 and 19.

To be certain that the microjet wall boundary condition in the numerical simulations is not artificially influencing the integration surface on which the drag is calculated, we carry out a control volume analysis[50] for the airfoil at $\alpha = 0°$ and microjet $C_\mu = 0.01$. Far-field integrations are performed at distances of 0.3c, 0.5c, and 0.7c, from the airfoil surface. Data presented in Table 7 suggests that the difference between the control-volume and surface-integrated drag coefficients grows slightly for the pressure side microjet as we move away from the surface likely due to the numerical errors. However, the difference between the integrated drag value at 0.7c away from the surface compared to the value at the surface is very small; about one drag count for the baseline (no jet) and about three drag counts for the airfoil with pressure side microjet. We see this as a verification of the numerical approach, and that the numerical model of the surface is not affected by the microjet wall boundary condition.

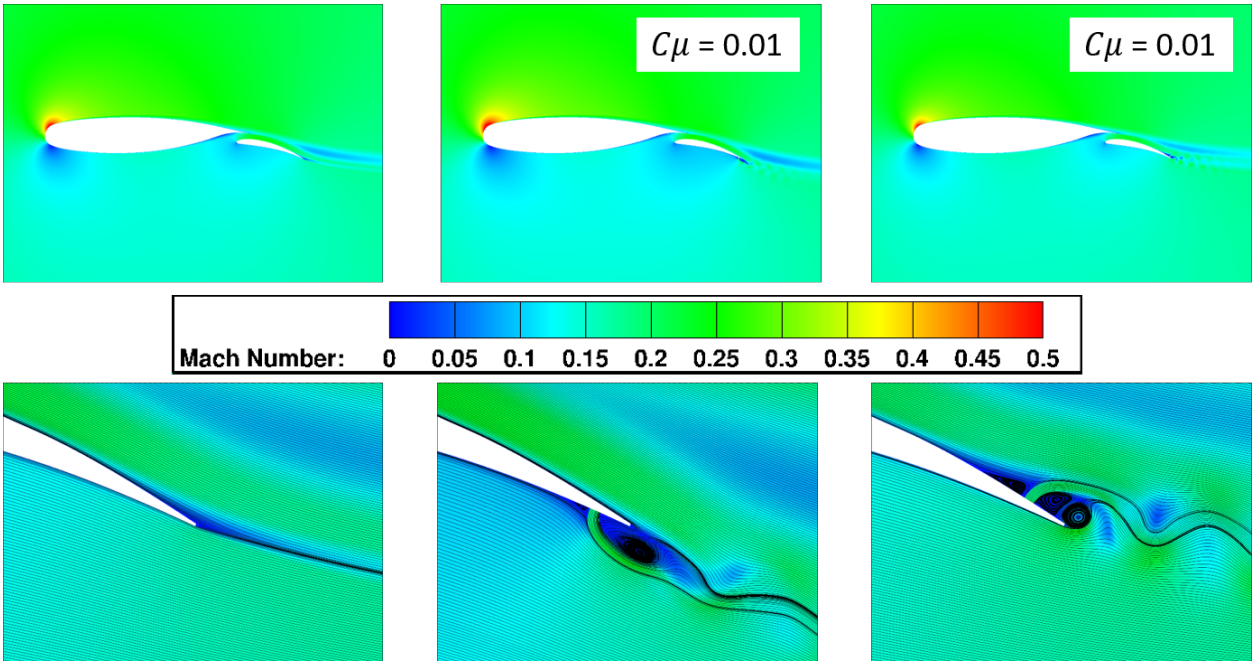

Figure 22: Flow visualization at $\alpha = 6°$ of microjet on the baseline, pressure side and suction side (left to right).

Table 7: Inspection of the drag coefficient at $\alpha = 6°$.

Case	Integration at	C_l	C_d
Baseline (no jet)	surface	1.624	0.01985
Baseline (no jet)	0.3c far-field	1.624	0.01979
Baseline (no jet)	0.5c far-field	1.624	0.01978
Baseline (no jet)	0.7c far-field	1.624	0.01977
Pressure side jet	surface	1.979	0.02285
Pressure side jet	0.3c far-field	1.980	0.02289
Pressure side jet	0.5c far-field	1.980	0.02304
Pressure side jet	0.7c far-field	1.982	0.02318

To explain the effects on the drag force, we compare the drag components of the airfoil with microjets on the pressure and suction side to the baseline airfoil with no microjet. We start from the mathematical equation for the drag force which can be derived using control volume analysis on the airfoil surface (see Equation 3).

$$F = \int \sigma_{ij} n_j dA + \int \rho u_i u_j n_j dA$$
$$\sigma_{ij} = -p\delta_{ij} + \tau_{ij} \tag{3}$$

$$D = F_x cos\alpha + F_z sin\alpha \tag{4}$$

δ_{ij} is the Kronecker delta, p is the pressure, τ_{ij} is the viscous stress tensor, α is the angle of attach, n_j is unit surface normal, and F_x and F_z are computed from x and z components of the force given in Equation 3. The first term in Equation 3 corresponds to the pressure and viscous terms and the second term corresponds to the momentum term. For conventional airfoil studies, the drag force is only dependent on the pressure and viscous terms as there is no momentum transfer through the airfoil surface. However, in this study,

the microjet injects momentum through the surface and therefore we must account for the momentum contribution to the overall drag value.

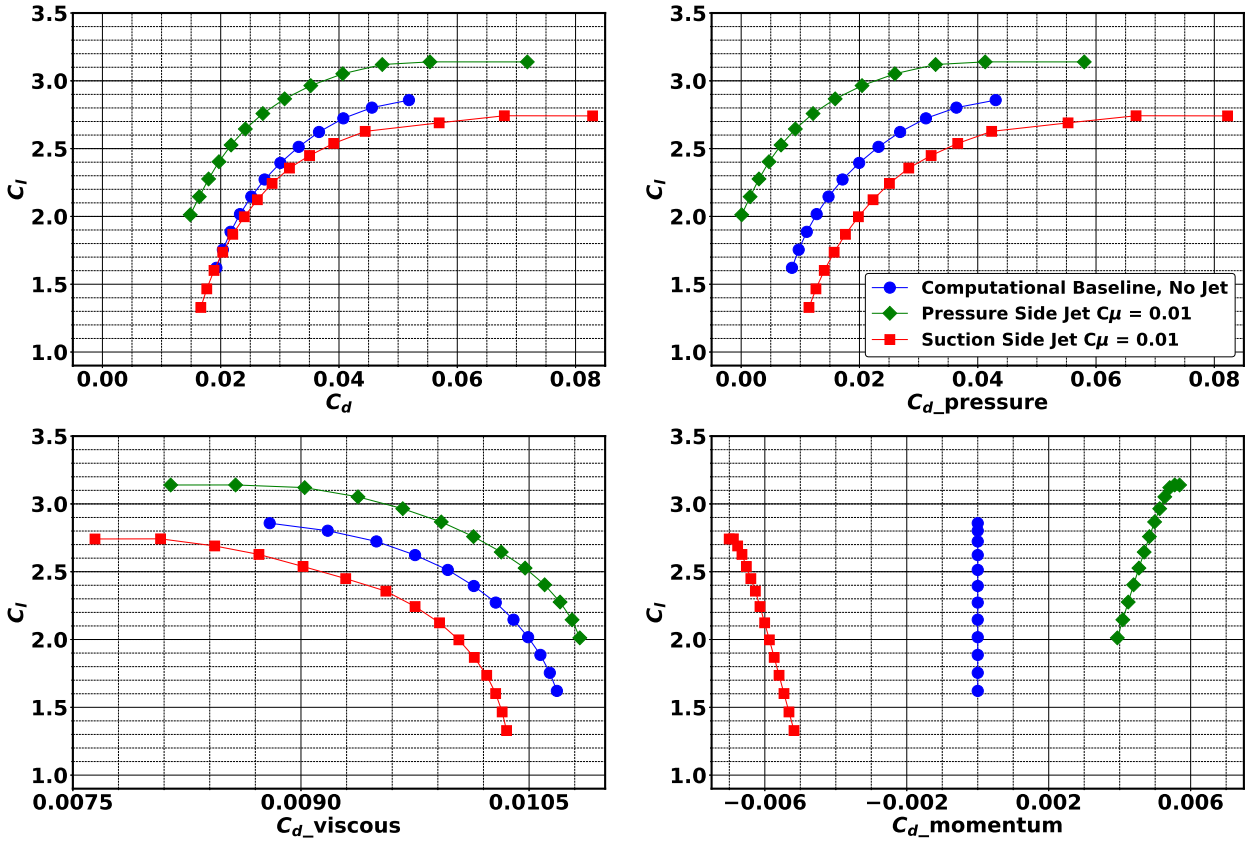

Figure 23: Drag decomposition study for the microjet with $C_\mu = 0.01$ on the pressure and suction side compared to the baseline. a) reports total drag polar, b) reports pressure drag polar, c) reports viscous drag polar, and d) reports momentum drag polar.

Utilizing Equation 3, we conduct a drag decomposition study in terms of drag coefficient polars to understand the microjet effect on each drag component for a given lift coefficient (see Figure 23). In Figure 23a we observe that for a given lift coefficient, $C_l = 2.50$, the total drag coefficient corresponding to the airfoil with pressure side microjet is 113 drag counts lower compared to the baseline (no jet), and the drag coefficient corresponding to the airfoil with suction side microjet is 41 drag counts higher than the baseline (no jet). The analysis indicates that the drag effect is mainly due to the change in the pressure distribution. Figure 22 shows that for the pressure side microjet, the drag component of the momentum injection is pointed upstream, and therefore, the corresponding momentum drag is positive (drag increases), and vice versa for the suction side microjet. In both cases, the change in the pressure drag is one order of magnitude larger than the changes in viscous or momentum drag as shown in Figure 23. For the airfoil with pressure side microjet, the pressure drag reduction far exceeds the viscous and momentum drag it adds. Therefore, the nominally-orthogonal microjet introduced in this study is an effective active flow control method and, when applied on the airfoil flap trailing edge pressure side, can potentially improve both lift and drag characteristic of high-lift systems.

IV. Conclusions

In this study we demonstrate with CFD the effectiveness of nominally-orthogonal jets as applied close to the flap trailing edge of a multi-element airfoil, NLR7301. We confirm that for high-lift applications, nominally-orthogonal jets can be an alternative to nominally-orthogonal physical tabs providing similar lift-enhancement opportunities. We investigate the effect of various nominally-orthogonal jet momentum

coefficients as applied to the airfoil's pressure side, and present the lift enhancement relationship $\Delta C_l \simeq 3.59\sqrt{(C_\mu)}$ for this flapped airfoil. We observe marginal gains in lift at high C_μ values, thus we put the emphasis of our study on a nominally-orthogonal jet with $C_\mu = 0.01$. We study the nominally-orthogonal jet effects as applied to the pressure and suction side individually. We show that the high-lift characteristics of the studied airfoil improve significantly using nominally-orthogonal jets applied near the trailing edge on either side of the airfoil. We show that a nominally-orthogonal jet with $C_\mu = 0.01$ at $95\%c_{flap}$ can successfully shift the lift curve of the multi-element airfoil up by $\Delta C_l = 0.36$ and down by $\Delta C_l = -0.27$ when employed on the pressure and suction sides, respectively. Further, a drag decomposition analysis explains the drag reduction observed in our results as well as by Malavard et al.[1] For a given lift coefficient, $C_l = 2.50$, the microjet can reduce the drag coefficient by 113 counts and increase the drag coefficient by 41 drag counts when employed on the pressure and the suction side, respectively, compared to the baseline (no jet). For the presented microjet study, the lift and drag decomposition studies suggest that the change in the lift and drag coefficients is largely due to changes in the pressure field and not directly a result of the added momentum. The lift increment and the drag decrement by the altered pressure field is found to be two and one orders of magnitude, respectively, greater than the changes due to the added momentum. In this study, we demonstrate that small trailing edge nominally-orthogonal jets can produce large, controllable and favorable changes in aerodynamic characteristics of an airfoil. This encourages future research and development opportunities in using nominally-orthogonal jets as effective active flow control devices. Future research will include sensitivities of the aerodynamic performance and loads to steady vs. impulsed microjets and also microjet chordwise location and jet slot size.

V. Acknowledgment

The research reported in this paper was partially funded by Boeing Commercial Airplanes (BCA), The Boeing Company. The computing resources were provided by the NASA Ames Research Center (ARC). The authors acknowledge the help and inputs by Dr. Paul Vijgen, BCA, and Dr. William Chan and Dr. H. Dogus Akaydin, NASA ARC.

References

[1]Malavard, L., Poisson-Quinton, P., and Jousserandot, P., "Theoretical and experimental investigations of circulation control," Tech. rep., Princeton University Department of Aeronautical Engineering, 1956.

[2]Blaylock, M., Chow, R., and van Dam, C. P., "Comparison of microjets with microtabs for active aerodynamic load control," *5th Flow Control Conference*, Paper#2005-1185, Chicago, Illinois, 2010.

[3]Blaylock, M., Chow, R., Cooperman, A., and van Dam, C. P., "A simple atmospheric boundary layer model applied to large eddy simulations of wind turbine wakes," *Wind Energy*, Vol. 17, 2014, pp. 657–669.

[4]Smith, A., "High-lift aerodynamics," *J.Aircraft*, Vol. 12, No. 6, 1975, pp. 501–530.

[5]van Dam, C. P., "The aerodynamic design of multi-element high-lift systems for transport airplanes," *Progress in Aerospace Sciences*, Vol. 38, No. 2, 2002, pp. 101–144.

[6]Meredith, P., "Viscous phenomena affecting high-lift systems and suggestions for future CFD development," *High-lift System Aerodynamics AGARD CP 515*, 1993, pp. 19(1)–19(8).

[7]Seifert, A., Bachar, T., Koss, D., Shepshelovich, M., and Wygnanski, I., "Oscillatory blowing: a tool to delay boundary-layer separation," *AIAA Journal*, Vol. 31, No. 11, 1993, pp. 2052–2060.

[8]Kühn, T., Ciobaca, V., Rudnik, R., Golling, B., and Breitenstein, W., "Active flow separation control on a high-lift wing-body configuration part 1: baseline flow and constant blowing," *29th AIAA Applied Aerodynamics Conference*, Paper#2011-3168, Honolulu, Hawaii, 2011.

[9]Ciobaca, V., Rudnik, R., Haucke, F., and Nitsche, W., "Active flow control on a high-lift airfoil: URANS simulations and comparison with time-accurate measurements," *31st AIAA Applied Aerodynamics Conference*, Paper#2013-2795, San Diego, CA, 2013.

[10]Ciobaca, V. and Wild, J., "Active flow control for an outer wing model of a take-off transport aircraft configuration - a numerical study," *32nd Applied Aerodynamics Conference*, Paper#2014-2403, Atlanta, GA, 2014.

[11]Kral, L. D., "Active flow control technology," *ASME Fluids Engineering Division Technical Brief*, 1998.

[12]Selby, G. V., Lin, J. C., and Howard, F. G., "Control of low-speed turbulent separated flow using jet vortex generators," *Experiments in Fluids*, Vol. 12, No. 6, 1992, pp. 394–400.

[13]Barrett, R. and Farokhi, S., "Subsonic aerodynamics and performance of a smart vortex generator system," *Journal of Aircraft*, Vol. 33, No. 2, 1996, pp. 393–398.

[14]Moreau, E., "Airflow control by non-thermal plasma actuators," *Journal of Physics D: Applied Physics*, Vol. 40, No. 3, 2007, pp. 605–636.

[15]Greenblatt, D. and Wygnanski, I. J., "Control of flow separation by periodic excitation," *Progress in Aerospace Sciences*, Vol. 36, No. 7, 2000, pp. 487–545.

[16]James, R. D., Jacobs, J. W., and Glezer, A., "A round turbulent jet produced by an oscillation diaphragm," *Physics of Fluids*, Vol. 8, No. 9, 1996, pp. 2484–2495.

[17]Lin, J. C., "Review of research on low-profile vortex generators to control boundary-layer separation," *Progress in Aerospace Sciences*, Vol. 38, No. 4-5, 2002, pp. 389–420.

[18]Lengers, M., "Industrial assessment of overall aircraft driven local active flow control," *Proceedings of the 29th Congress of the International Council of the Aeronautical Sciences*, St. Petersburg, Russia, 2014.

[19]Shmilovich, A. and Yadlin, Y., "Active Flow control for practical high-lift systems," *Journal of Aircraft*, Vol. 46, No. 4, 2009, pp. 1354–1364.

[20]Desalvo, M., Whalen, E., and Glezer, A., "High-lift enhancement using active flow control," *6th AIAA Flow Control Conference*, Paper#2012-3245, New Orleans, Louisiana, 2012.

[21]Eggert, C. A. and Rumsey, C. L., "CFD study of NACA 0018 airfoil with flow control," *NASA STI Program*, 2017.

[22]Shmilovich, A., Yadlin, Y., and Whalen, E., "Computational evaluation of flow control for enhanced control authority of a vertical tail," *AIAA Journal*, Vol. 54, No. 8, 2016, pp. 2211–2220.

[23]Bauer, M., Lohse, J., Haucke, F., and Nitsche, W., "High-lift performance investigation of a two-element configuration with a two-stage actuator system," *AIAA Journal*, Vol. 52, No. 6, 2014, pp. 1307–1313.

[24]Wild, J., "Experimental investigation of Mach- and Reynolds-number dependencies of the stall behavior of 2-element and 3-element high-lift wing sections," *50th AIAA Aerospace Sciences Meeting including the New Horizons Forum and Aerospace Exposition*, Paper#2012-0108, Nashville, Tennessee, 2012.

[25]Englar, R. J., "Circulation control for high lift and drag generation on STOL aircraft," *Journal of Aircraft*, Vol. 12, No. 5, 1975, pp. 457–463.

[26]Kota, S., Hetrick, J. A., Osborn, R., Paul, D., Pendleton, E., Flick, P., and Tilmann, C., "Design and application of compliant mechanisms for morphing aircraft structures," *SPIE*, Vol. 5054, No. 734, 2003, pp. 24.

[27]Lee, H. and Kroo, I., "Computational investigation of airfoils with miniature trailing edge control surfaces," *42nd AIAA Aerospace Sciences Meeting and Exhibit*, Paper#2004-1051, Reno, Nevada, 2004.

[28]Baker, J. P., Standish, K. J., and van Dam, C. P., "Two-dimensional wind tunnel and computational investigation of a microtab modified S809 airfoil," *43rd AIAA Aerospace Sciences Meeting and Exhibit*, Paper#2005-1186, Reno, Nevada, 2005.

[29]Mayda, E. A., van Dam, C. P., and Nakafuji, D. Y., "Computational investigation of finite width microtabs for aerodynamic load control," *43rd AIAA Aerospace Sciences Meeting and Exhibit*, Paper#2005-1185, Reno, Nevada, 2005.

[30]Chow, R. and van Dam, C. P., "Unsteady computational investigations of deploying load control microtabs," *Journal of Aircraft*, Vol. 43, No. 5, 2006, pp. 1458–1469.

[31]Baker, J. P., Standish, K. J., and van Dam, C. P., "Two-dimensional wind tunnel and computational investigation of a microtab modified airfoil," *Journal of Aircraft*, Vol. 44, No. 2, 2007, pp. 563–572.

[32]Cooperman, A. M. and van Dam, C. P., "Closed-loop control of a microtab-based load control system," *Journal of Aircraft*, Vol. 52, No. 2, 2015, pp. 387–394.

[33]Ross, J. C., Storms, B. L., and Carrannanto, P. G., "Lift-enhancing tabs on multi-element airfoils," *11th AIAA Applied Aerodynamics Confrence*, Paper#93-3504, Monterey, California, 1993.

[34]Chow, R. and van Dam, C. P., "Computational investigations of deploying load control microtabs on a wind turbine airfoil," *45th AIAA Aerospace Sciences Meeting and Exhibit*, Paper#2007-1018, Reno, Nevada, 2007.

[35]Brunner, M. S., Blaylock, M., Cooperman, A. M., and van Dam, C. P., "Comparison of CFD with wind tunnel tests of microjets," *50th AIAA Aerospace Sciences Meeting including the New Horizons Forum and Aerospace Exposition*, Paper#2012-0898, Nashville, Tennessee, 2012, pp. 1–11.

[36]Cooperman, A. M., *Wind tunnel testing of microtabs and microjets for active load control of wind turbine blades*, Ph.D. thesis, University of California Davis, 2012.

[37]Vandenberg, B. and Oskam, B., "Boundary layer measurements on a two-dimensional wing with flap and a comparison with calculations," *In AGARD Turbulent Boundary Layers 14 p (SEE N80-27647 18-34)*, 1980.

[38]Suhs, N., Rogers, S., and Dietz, W., "PEGASUS 5: an automated pre-processor for overset-grid CFD," *32nd AIAA Fluid Dynamics Conference and Exhibit*, Paper#2002-3186, St. Louis, Missouri, 2002.

[39]Pulliam, T. H. and Chaussee, D. S., "A diagonal form of an implicit approximate-factorization algorithm," *Journal of Computational Physics*, Vol. 39, No. 2, 1981, pp. 347–363.

[40]Spalart, P. and Allmaras, S., "A one-equation turbulence model for aerodynamic flows," *La Recherche Aerospatiale*, Vol. 1, No. 1, 1994, pp. 5–21.

[41]Brodeur, R. R., *Boundary layer transition prediction for a two dimensional Reynolds averaged Navier-Stokes solver*, Ph.D. thesis, University of California Davis, 1997.

[42]Meakin, R., "Object x-rays for cutting holes in composite overset structured grids," *15th AIAA Computational Fluid Dynamic Conference*, Paper#2001-2537, Anaheim, CA, 2001.

[43]Tramel, R. W., Nichols, R. H., and Buning, P. G., "Addition of improved shock-capturing schemes to OVERFLOW 2.1," *19th AIAA Computational Fluid Dynamics Conference*, Paper#2009-3988, San Antonio, Texas, 2009.

[44]Beam, R. M. and Warming, R. F., "An implicit factored scheme for the compressible Navier-Stokes equations," *AIAA Journal*, Vol. 16, No. 4, 1978, pp. 393–402.

[45]Menter, F. R., "Two-equation eddy-viscosity turbulence models for engineering applications," *AIAA Journal*, Vol. 32, No. 8, 1994, pp. 1598–1605.

[46]Langtry, R. B. and Menter, F. R., "Correlation-based transition modeling for unstructured parallelized computational fluid dynamics codes," *AIAA Journal*, Vol. 47, No. 12, 2009, pp. 2894–2906.

[47]Nichols, R. H., "Turbulence models and their application to complex flows," *University of Alabama at Birmingham*, https://overflow.larc.nasa.gov/files/2014/06/Turbulence_Guide_v4.01.pdf.

[48]Pulliam, T. H., "Time accuracy and the use of implicit methods," *11th AIAA Computational Fluid Dynamics Conference*, Paper#93-3360, Orlando, Florida, 1993.

[49]Anderson Jr, J. D., *Fundamentals of aerodynamics*, Tata McGraw-Hill Education, 2010.

[50]van Dam, C. P., "Recent experience with different methods of drag prediction," *Progress in Aerospace Sciences*, Vol. 35, No. 8, 1999, pp. 751–798.